



# CHORUS

This is the accepted manuscript made available via CHORUS. The article has been published as:

## Type-II Dirac cones and electron-phonon interaction in monolayer biphenylene from first-principles calculations

Peng-Fei Liu, Jingyu Li, Chi Zhang, Xin-Hai Tu, Junrong Zhang, Ping Zhang, Bao-Tian Wang, and David J. Singh

Phys. Rev. B **104**, 235422 — Published 16 December 2021

DOI: [10.1103/PhysRevB.104.235422](https://doi.org/10.1103/PhysRevB.104.235422)

# Type-II Dirac Cones and Electron-Phonon Interactions in Monolayer Biphenylene from First-Principles Calculations

Peng-Fei Liu,<sup>1,2</sup> Jingyu Li,<sup>3,4</sup> Chi Zhang,<sup>5</sup> Xin-Hai Tu,<sup>1,2</sup> Junrong Zhang,<sup>1,2</sup> Ping Zhang,<sup>6,7</sup> Bao-Tian Wang,<sup>1,2,8,\*</sup> and David J. Singh<sup>9,10</sup>

<sup>1</sup>*Institute of High Energy Physics, Chinese Academy of Sciences, Beijing 100049, China*

<sup>2</sup>*Spallation Neutron Source Science Center, Dongguan 523803, China*

<sup>3</sup>*Key Laboratory of Materials Physics, Institute of Solid State Physics, HFIPS, Chinese Academy of Sciences, Hefei 230031, China*

<sup>4</sup>*Foshan (Southern China) Institute for New Materials, Foshan 528200, Guangdong, China*

<sup>5</sup>*College of Electrical Engineering, Henan University of Technology, Zhengzhou 450001, China*

<sup>6</sup>*School of Physics and Physical Engineering, Qufu Normal University, Qufu 273165, China*

<sup>7</sup>*LCP, Institute of Applied Physics and Computational Mathematics, Beijing 100088, China*

<sup>8</sup>*Collaborative Innovation Center of Extreme Optics, Shanxi University, Taiyuan, Shanxi 030006, China*

<sup>9</sup>*Department of Physics and Astronomy, University of Missouri, Columbia, Missouri 65211, USA*

<sup>10</sup>*Department of Chemistry, University of Missouri, Columbia, Missouri 65211, USA*

(Dated: December 8, 2021)

We report first principles investigation of electronic structure, topological bands and electron-phonon interactions in metallic biphenylene sheets. Biphenylene is a recently synthesized  $sp^2$ -bonded carbon allotrope. We find coupling of electrons at the Fermi surface to very high frequency carbon derived phonons, analogous to superconducting  $MgB_2$ . This leads to low temperature weak coupling superconductivity due to an unusual combination of exceptionally large logarithmically averaged phonon frequency  $\omega_{log}=1369$  K and moderate electron-phonon coupling. The electronic structure shows a two band Fermi surface dominated by C  $p_z$  orbitals and a pair of type-II tilted Dirac cones along the  $\Gamma$ -Y line at the Brillouin zone boundary. Berry curvature and edge state calculations show that monolayer biphenylene is a two dimensional  $\mathbb{Z}_2$  topological material. Thus monolayer biphenylene is predicted to be a topological superconductor based on C  $p$  orbitals and high frequency phonons.

## I. INTRODUCTION

Carbon is exceptional in the diversity of its allotropes arising from its combination of strong directional covalent bonding and competition between different hybridization schemes, particularly  $sp$ ,  $sp^2$  and  $sp^3$  bonding<sup>1</sup>. The strong bonding leading to highly dispersive energy bands and generally high stability of the allotropes has provided exciting platforms for realizing novel physics. These include graphite<sup>2</sup>, diamond<sup>3</sup>, carbon nanotubes<sup>4</sup>, fullerenes<sup>5</sup>, graphene<sup>6</sup>, and others<sup>1</sup>. Graphene in particular provides a platform for a wide variety of novel behaviors associated with its Dirac cones at the Fermi level<sup>6,7</sup>. These include ballistic charge transport<sup>8</sup>, the quantum spin Hall effect<sup>9</sup>, Klein tunneling<sup>10</sup>, exceptional carrier mobilities<sup>11</sup>, Majorana zero modes<sup>12</sup>, and other phenomena<sup>13</sup>. This motivates searches for and investigation of other Dirac materials<sup>14-18</sup>, especially materials based on carbon and analogues of them.

Carbon based superconductivity provides the possibility of exceptionally high critical temperatures due to the possibility of coupling to high frequency phonons with strong electron-phonon matrix elements arising from the strong bonding and light mass of carbon, as well as the possibility of novel features associated with topological aspects of the electronic structure of some carbon allotropes especially graphene. This was anticipated in the discovery of electron-phonon superconductivity  $MgB_2$ , which is closely related to graphene.  $MgB_2$  has an exceptionally high ambient pressure critical temperature of  $T_c=39$  K<sup>19</sup>, based on coupling to high frequency modes as well as two gap superconductivity<sup>20,21</sup>. In fact,

the unique carbon-like characteristics of  $MgB_2$ , specifically high energy scales has enabled elucidation of two gap superconducting physics<sup>22</sup>. Additionally, similar and higher critical temperatures have been discovered in doped fullerenes, which in addition provide a platform for investigating superconductivity in proximity to metal insulator transitions and magnetism<sup>23</sup>. Finally, graphene itself has been shown to be an exciting superconductor when modified through doping or through twisting<sup>24-32</sup>. Superconductivity with  $T_c \sim 5.9$  K is found Li-decorated monolayer graphene<sup>33</sup>. Superconductivity has also been observed in Ca-decorated graphene<sup>34,35</sup>. First principles theory shows that these are well explained as electron-phonon superconductors<sup>28,36,37</sup>.

These results raise the question of whether an intrinsic a 2D  $sp^2$ -bonded carbon allotrope with topological Dirac cones and superconductivity without requiring doping, twisting or strain can be found. This would offer the potential for a highly stable, readily realizable platform for investigating topological superconductivity. Here we investigate biphenylene as a candidate and find that it is in fact a topological superconductor, with features related to those of  $MgB_2$ , particularly the coupling to high frequency phonons, but in a weak coupling regime.

Biphenylene is a planar  $sp^2$ -hybridized carbon allotrope with intrinsic Dirac cones. Similar to graphene, it is atomically thin. However, the structure is more complex, and is comprised of approximately square four membered, six membered, and eight membered carbon rings<sup>38</sup>. The possibility of synthesizing biphenylene has been recognized for some time. This motivated several attempts and synthesis and the

discovery of interesting related phases with potential practical applications<sup>39–41</sup>. Finally, biphenylene was recently experimentally synthesized<sup>42</sup>, and shown to be a stable metal<sup>43–45</sup>. Here we show that besides being a metal, biphenylene is both a topological metal and superconducting. We find that there is a pair of type-II Dirac cones derived from C  $p_z$  orbitals approximately 0.63 eV above the Fermi energy in monolayer biphenylene and that the material is an electron-phonon superconductor. It exhibits a nontrivial  $\mathbb{Z}_2$  topological invariant exhibiting protected edge states at the boundaries with one-way propagation.

## II. COMPUTATIONAL METHODS

Our first principles calculations were performed in density functional theory (DFT) with the local density approximation (LDA) and norm-conserving pseudopotentials<sup>46,47</sup>. We used a planewave basis as implemented in the Quantum-ESPRESSO (QE) package<sup>48,49</sup>, with planewave basis set cutoffs of 80 Ry for the wave functions and 320 Ry for the charge density. The zone sampling in the self-consistent calculations was done with a Methfessel-Paxton smearing of 0.02 Ry on a  $20 \times 16$  Monkhorst-Pack grid  $\mathbf{k}$ -mesh<sup>50</sup>. The internal atomic positions are fully relaxed with a threshold of 10 meV/Å for the forces. We used periodic supercells with a length of 20 Å along the  $z$ -direction, perpendicular to the biphenylene sheets.

The phonon dispersions were calculated within density functional perturbation theory<sup>51</sup> on a  $10 \times 8$   $\mathbf{q}$ -mesh using the Phonon code in the QE package. The mode-resolved magnitudes of the electron phonon coupling (EPC)  $\lambda_{\mathbf{q}\nu}$  were calculated as<sup>52,53</sup>

$$\lambda_{\mathbf{q}\nu} = \frac{\gamma_{\mathbf{q}\nu}}{\pi \hbar N(E_F) \omega_{\mathbf{q}\nu}^2}, \quad (1)$$

where  $\gamma_{\mathbf{q}\nu}$  is the phonon linewidth,  $\omega_{\mathbf{q}\nu}$  is the phonon frequency, and  $N(E_F)$  is the electronic density of states at the Fermi level. The  $\gamma_{\mathbf{q}\nu}$  are

$$\gamma_{\mathbf{q}\nu} = \frac{2\pi\omega_{\mathbf{q}\nu}}{\Omega_{\text{BZ}}} \sum_{\mathbf{k}, n, m} |g_{\mathbf{k}\mathbf{n}, \mathbf{k}+\mathbf{q}\mathbf{m}}^\nu|^2 \delta(\varepsilon_{\mathbf{k}\mathbf{n}} - \varepsilon_F) \delta(\varepsilon_{\mathbf{k}+\mathbf{q}\mathbf{m}} - \varepsilon_F), \quad (2)$$

where  $\Omega_{\text{BZ}}$  is the volume of the Brillouin zone, the  $\varepsilon_{\mathbf{k}\mathbf{n}}$  ( $\varepsilon_{\mathbf{k}+\mathbf{q}\mathbf{m}}$ ) are the Kohn-Sham eigenvalues, and  $g_{\mathbf{k}\mathbf{n}, \mathbf{k}+\mathbf{q}\mathbf{m}}^\nu$  are the EPC matrix elements<sup>54</sup>. The Eliashberg electron-phonon spectral function  $\alpha^2 F(\omega)$  is then calculated by

$$\alpha^2 F(\omega) = \frac{1}{2\pi N(E_F)} \sum_{\mathbf{q}\nu} \frac{\gamma_{\mathbf{q}\nu}}{\omega_{\mathbf{q}\nu}} \delta(\omega - \omega_{\mathbf{q}\nu}). \quad (3)$$

The total EPC  $\lambda$  can be calculated in two ways. These are integration of the EPC constant  $\lambda_{\mathbf{q}\nu}$  in the full Brillouin zone for all phonon modes or by integrating the Eliashberg spectral function  $\alpha^2 F(\omega)$ <sup>55</sup>

$$\lambda(\omega) = \sum_{\mathbf{q}\nu} \lambda_{\mathbf{q}\nu} = 2 \int_0^\omega \frac{\alpha^2 F(\omega)}{\omega} d\omega. \quad (4)$$

The superconducting transition temperature,  $T_c$ , is determined from the calculated EPC constant  $\lambda$  by the McMillan-Allen-Dynes formula,

$$T_c = f_1 f_2 \frac{\omega_{\text{log}}}{1.2} \exp \left[ -\frac{1.04(1 + \lambda)}{\lambda - \mu^*(1 + 0.62\lambda)} \right], \quad (5)$$

where  $\mu^*$  is the effective screened Coulomb repulsion constant,  $\omega_{\text{log}}$  is the logarithmic average frequency,

$$\omega_{\text{log}} = \exp \left[ \frac{2}{\lambda} \int_0^\infty \frac{d\omega}{\omega} \alpha^2 F(\omega) \log \omega \right], \quad (6)$$

and  $f_i$  is the correction factor when  $\lambda > 1.3$ <sup>56</sup>. As discussed below, we find lower values of  $\lambda$  characteristic of weak coupling, and used values of  $\mu^* = 0.1$  and  $f_1 f_2 = 1$ .

We analyzed the electronic structure in terms of Wannier orbitals in order to examine the electronic structure of nanoribbons for edge states. The Wannier tight-binding (TB) Hamiltonian was constructed from the first principles Bloch functions by projecting the states onto maximally localized Wannier functions (MLWFs)<sup>57</sup> using the Wannier90 package<sup>58,59</sup>. In the model, the MLWFs are derived from six C  $p_z$  orbitals. The nontrivial boundary-edged states are calculated from the imaginary part of the surface Green's function<sup>60</sup> as obtained with the WannierTools package<sup>61</sup>. Fermi surfaces colored as a function of an arbitrary scalar quantities in this work are drew by using the FermiSurfer program<sup>62</sup>.

## III. RESULTS AND DISCUSSION

### A. Atomic structure and electronic properties

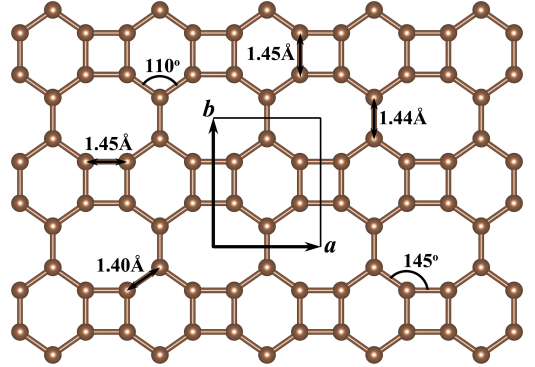


FIG. 1. Structure of monolayer biphenylene in a top view. The unit cell, bond lengths, and angles are as indicated by the solid black lines.

Layered biphenylene forms in the centrosymmetric orthorhombic space group  $Pmmm$  (No. 47). The monolayer is illustrated in Fig. 1. There are two crystallographically distinct C positions: C1, site symmetry  $4z$  and C2, site symmetry  $2p$ . The optimized lattice constants are  $a=3.75$  Å and  $b=4.51$  Å. These compare well with a prior calculation ( $a=3.76$  Å and

$b=4.52 \text{ \AA}$ )<sup>38</sup>. Importantly, the structure is clearly anisotropic between the  $a$  and  $b$  directions. This leads to the expectation of anisotropic physical properties. The structure is based on three types of C rings: tetragons hexagons and octagons, with C-C bond lengths ranging from 1.40  $\text{\AA}$  to 1.45  $\text{\AA}$ , similar to the value of 1.42  $\text{\AA}$  in graphene. All the C atoms are threefold coordinated as expected for  $sp^2$  hybridization, but the angles vary with values of 90°, 110°, 125°, and 145°. We find that relaxations starting with imposed buckling of the sheets invariably returned to the planar unbuckled 2D structure. This shows that monolayer biphenylene has a truly planar structure.

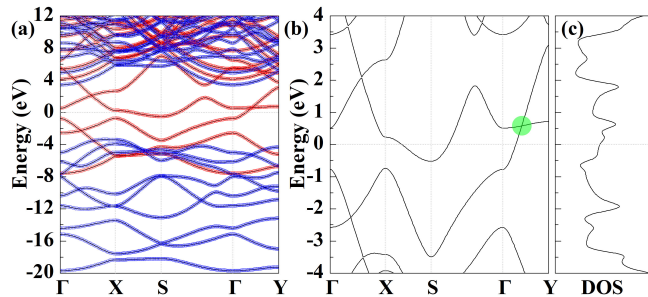


FIG. 2. (a) Calculated orbital-resolved band structures of a biphenylene monolayer. The red and blue circles highlight the  $\pi$  and  $\sigma$  bands arising from  $p_z$  and  $sp^2$ -hybrid orbitals, respectively. The high-symmetry points,  $\Gamma$ , X, Y, and S are (0,0), (1/2,0), (0,1/2), and (1/2,1/2), respectively. The Fermi level is set to zero. (b) Band structure of monolayer biphenylene around the Fermi level, showing the Dirac cone marked by a green circle. (c) Calculated electronic density of states in the energy region of the band structure of (b).

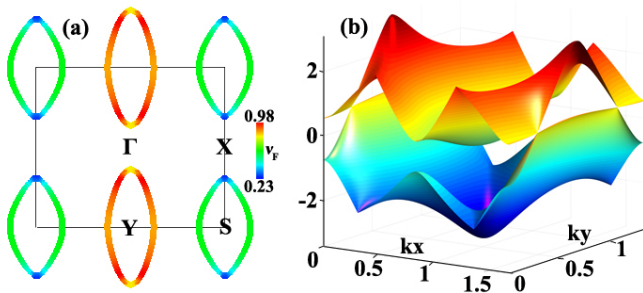


FIG. 3. (a) The 2D Fermi surface formed by the two bands that cross the Fermi level, colored to indicate relative Fermi velocity. The red, green, and blue regions have high, middle, and low Fermi velocity  $v_F$ , respectively. (b) Three-dimensional visualization of the type-II Dirac cones.

The calculated band structure and corresponding electronic density of states are shown in Fig. 2. The band structure is metallic with two bands crossing the Fermi level. This is in accord with prior calculations<sup>38,63</sup> and experimental  $dV/dI$  spectra<sup>42</sup>. As shown in the orbital-resolved band structure of Fig. 2a, the  $p_{x,y}$  orbitals hybridize with the  $s$  orbitals to form 18 strong covalent in-plane  $\sigma$  bonds. The unhybridized  $p_z$  orbitals form six relatively weak out-of-plane  $\pi$  bonds. The third and fourth  $\pi$  bands contribute to the Fermi surface. Thus the Fermi surface is derived from  $\pi$  orbitals. As seen, the valence

and the conduction bands touch along the  $\Gamma$ -Y line with linear dispersion to form intrinsic type-II Dirac cones approximately 0.63 eV above the Fermi level (Figs. 2b and 3b). Also, as seen in Fig. 3a, the valence band contributes elliptical hole pockets around Y, while the conduction band forms elliptical electron pockets around the S points. Thus the Fermi surface has two Fermi pockets. These Fermi surfaces are compensating with equal areas corresponding to the even electron count, but have different average velocities.

The Fermi surfaces colored to indicate relative Fermi velocity are shown in Fig. 3a. The ratio between the maximum and minimum velocity is approximately 4.2. This reflects the very different slopes of the bands comprising the Fermi surface as seen in the band structure, for example the high velocity of the lower band coming from  $\Gamma$  and crossing the Fermi level along  $\Gamma$ -Y, as compared to the relatively weak dispersion of the band crossing the Fermi level along X-S. Thus the hole pocket around Y has higher Fermi velocity than the electron pocket around S, leading to the expectation that the electrical transport will be dominated by hole carriers, while the density of states will be dominated by the electron carriers. This is opposite to the iron based superconductors and many other superconductors where hole Fermi surfaces are heavier than the electron Fermi surfaces in terms of Fermi velocities<sup>64</sup>. We note that, similar to graphene, spin orbit is expected to have an extremely small effect as a consequence of the small atomic number of carbon<sup>65,66</sup>.

## B. Topological numbers and edge states

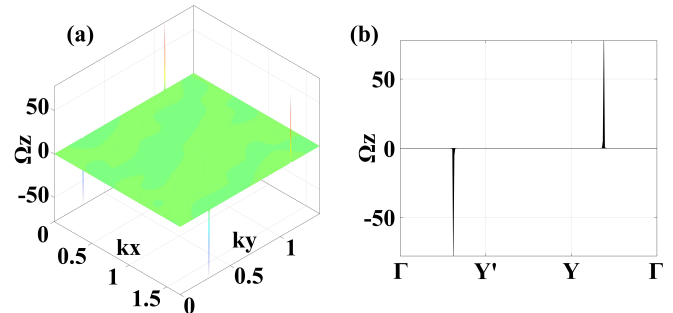


FIG. 4. Berry curvature  $\Omega_z$  distributions (a) in the Brillouin zone and (b) along the high-symmetry lines for single-layer biphenylene.

As may be noted, graphene, which is a Dirac material, has an intrinsic nontrivial topological band feature<sup>9</sup>. Especially in light of this it is important to determine whether 2D biphenylene with its Dirac cones is also topological. Biphenylene has a structure with inversion symmetry. Therefore we can verify the nontrivial topological nature of a biphenylene sheet via the  $\mathbb{Z}_2$  topological invariant. This number comes directly from the parities of the occupied bands at time reversal invariant momentum (TRIM) points<sup>67,68</sup>. The parities  $\xi(i)$  of twelve occupied valence bands for the biphenylene monolayer are given in Table I. The parity products for the occupied states at the TRIM points are calculated, by  $\delta(k_i) = \prod_{N=1}^{12} \xi(i)$ , to be +1,



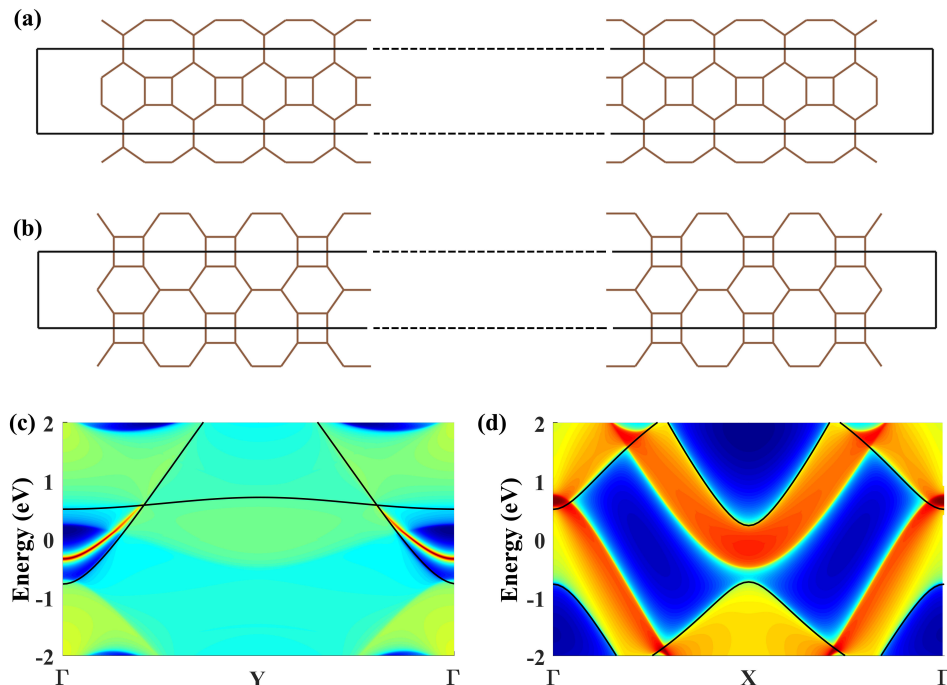


FIG. 5. Structural models for ribbons of single-layer biphenylene with (a) armchair-edged and (b) zigzag-edged boundaries. To clearly display the nanoribbons, we replace some of the repeated periodic cells by dotted lines. Momentum resolved local density of states projected on the edges of semi-infinite nanoribbons for (c) armchair and (d) zigzag boundaries. The black lines in (c) and (d) indicate the band structure of monolayer biphenylene.

+1, -1 and +1 for  $\Gamma$ , X, Y, and S, respectively. This yields a nontrivial topological invariant  $\nu = 1$  by  $(-1)^\nu = \prod_{i=1}^4 \delta(k_i)$ . This result clearly indicates the presence of non-trivial topological states in biphenylene.

TABLE I. The calculated parity eigenvalues of the twelve occupied spin-degenerate bands at four TRIM points for monolayer biphenylene.

TRIM	Parities	Product
$\Gamma$	++--+-+--+-	+
X	-+-+--++--+-	+
Y	+--+-+--+-+--	-
S	-+-+--++--+-	+

To further confirm the topological nature of the Dirac points, we calculate the Berry curvature<sup>69</sup> via

$$\Omega_n^z(\mathbf{k}) = i \langle u_n(\mathbf{k}) | \nabla_{\mathbf{k}} | u_n(\mathbf{k}) \rangle, \quad (7)$$

where  $u_k(\mathbf{k})$  represents the Bloch wave function of the  $n$ -th band. In Fig. 4, a pair of Dirac points at the boundary of the Brillouin zone could show the positive and negative Berry curvature distributions. These then would serve as the source and sink of the Berry curvature in the momentum space, respec-

tively. We calculate the Berry phases<sup>69,70</sup> by

$$\gamma_n = \oint_C \Omega_n^z(\mathbf{k}) \cdot d\mathbf{k}. \quad (8)$$

For this purpose, we define a circle on the  $\mathbf{k}_z = 0$  plane centered at the Dirac point to calculate the Berry phase<sup>71</sup>. The needed radius of the circle is arbitrary as long as it does not cover another Dirac point. We find that the Berry phase for the Dirac point is either  $\pi$  or  $-\pi$ , indicating that the crossing points are indeed pairs of topologically nontrivial points with opposite Berry phases<sup>69</sup>.

Nontrivial topology in a 2D crystal can be also characterized via the topologically protected edge states due to the bulk-edge correspondence<sup>72,73</sup>. We used a TB model as mentioned above to construct a supercells of a one-dimensional nanoribbons. As discussed in the case of graphene<sup>73</sup>, two representative nanoribbons, one with a zigzag configuration shown in Fig. 5a and one with an armchair configuration shown in Fig. 5b were constructed by cutting the biphenylene sheet. For the armchair-edged boundary, as shown in Fig. 5c, the topologically protected edge states originate from the Dirac points and disappear into the bulk states. This confirms the nontrivial topological phase in monolayer biphenylene. In the case of the zigzag-edged ribbon, as indicated in Fig. 5d, we find an absence of  $(d-1)$ -dimensional edge states. This is consistent with the above topological chirality analysis where only the Y point hosts odd parity and gives rise to the topological band.

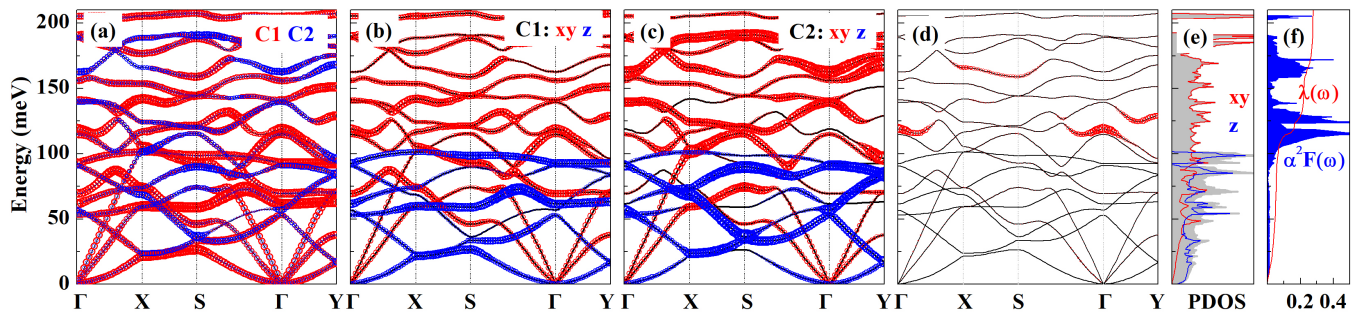


FIG. 6. (a-c) Calculated phonon spectra for the biphenylene monolayer highlighting the primary nature of the different modes. C1 and C2 are the C atoms with site symmetry  $4z$  and  $2p$ , respectively.  $xy$  shown as red are in-plane vibrations, and  $z$  shown as blue are out-of-plane vibrations. (d) Calculated phonon dispersions for monolayer biphenylene with the size of red circles being proportional to the magnitude of  $\lambda_{q\nu}$ . (e) Projected phonon density of states. (f) Frequency-dependent Eliashberg spectral function  $\alpha^2F(\omega)$  and cumulative frequency-dependent EPC function  $\lambda(\omega)$ .

### C. Phonons and electron-phonon interactions

Figure 6 shows the phonon dispersions and the projected phonon density of state (PhDOS) over the whole frequency range. The results are in accord with prior calculations<sup>38,63,74,75</sup>. The absence of unstable modes in the Brillouin zone confirms the dynamic stability of monolayer biphenylene with a planar structure. The highest phonon frequency is approximately 209 meV, which is slightly larger than in the case of graphene<sup>71</sup>. There are six atoms per unit cell in biphenylene leading to eighteen phonon branches in the dispersion: three acoustic and fifteen optical branches. The acoustic branches are an out-of-plane (ZA), an in-plane transverse (TA) and an in-plane longitudinal (LA) branch. These cross several low-frequency optical branches. The ZA mode around the  $\Gamma$  point has a parabolic dispersion characteristic of a planar material, while the LA and TA modes show linear dispersions near the  $\Gamma$  point.

We used in-house post-processing programs to determine atomic characters and directions<sup>76,77</sup> based on  $|e_\nu^\alpha(j, \mathbf{q})|^2$ , where  $e$  is the polarization vector of the  $j$ -th atom and the  $\nu$ -th band at  $\mathbf{q}$  along the  $\alpha$  direction. The phonon dispersions colored according to the contributions of different C sites and vibrational directions are shown in Figs. 6a, 6b and 6c. The out-of-plane C vibrations mainly contribute to the lower energy phonons. The high-energy phonons, above 100 meV, are almost entirely from the in-plane vibrations. This is similar to graphene.

We now turn to superconductivity, which we discuss based on the calculated electron-phonon Eliashberg spectral function  $\alpha^2F(\omega)$ . As seen in Fig. 6d, phonons from 119 to 130 meV, dominated by the in-plane vibrations that modulate C-C bond lengths, make the main contributions to the EPC based on the calculated  $\alpha^2F(\omega)$ . There are also significant contributions from even higher frequency modes as seen in the peak in the spectral function around 150 meV. This is different from the behavior of most other 2D superconductors, such as  $\text{Cu}_2\text{Si}$ <sup>78</sup>, borophene<sup>79</sup>,  $\text{B}_2\text{O}$ <sup>80</sup> and Cu-BHT<sup>81</sup>. In those materials out-of-plane vibrations dominate the EPC.

The integrated EPC  $\lambda_{tot}(\mathbf{q})$ , given by  $\lambda_{tot}(\mathbf{q}) =$

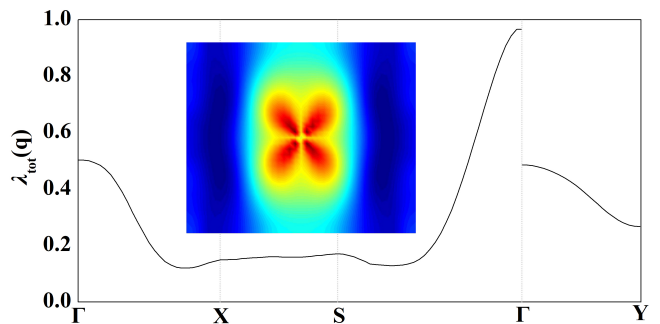


FIG. 7. The integrated EPC  $\lambda_{tot}(\mathbf{q})$  distributions (a) in the Brillouin zone and (b) along the high-symmetry directions.

$\sum_\nu \lambda_\nu(\mathbf{q})$ , is plotted in Fig. 7. According to the Eq. 1, when  $\omega_{q\nu}^2$  is zero,  $\lambda_{q\nu}$  goes to infinity. To make it sense, we set the  $\lambda_{q\nu}$  of the three acoustic branches at the  $\Gamma$  point to the nearest neighbor. As seen, optical phonons around the  $\Gamma$  point contribute strongly to the EPC. This is seen particularly along the  $\Gamma$ -S line. The overall EPC constant  $\lambda$  is approximately 0.3. This is a very small value for a superconductor. Nonetheless, superconductivity with a  $T_c$  of 0.59 K is predicted with  $\mu^*=0.1$ . The relatively high  $T_c$  for low  $\lambda$  is a consequence of the very high frequencies of the phonons that are coupled. The logarithmic averaged frequency  $\omega_{log}$  for biphenylene sheet is 1369 K. The critical temperature is larger than that predicted in hole doped graphene<sup>30</sup>, where  $\lambda = 0.27$  and  $T_c$  in the order of  $\sim 10^{-4}$  K were reported. It is also much smaller than the values ( $\lambda = 0.55$  and  $T_c = 5.1$ -7.6 K) in Li-decorated graphene<sup>28</sup>, ( $\lambda = 0.71$  and  $T_c = 6.8$ -8.1 K) in Ca-intercalated graphene<sup>36</sup>, and ( $\lambda = 0.42$  and  $T_c = 13$  K) in heavily  $n$ -doped graphene<sup>30</sup>. The logarithmic averaged frequency  $\omega_{log}$  for biphenylene sheet is comparable to the value of  $\omega_{log}=1316$  K in hole doped graphene<sup>30</sup>. This implies an analogy between the superconductivity of hole doped graphene and intrinsic undoped biphenylene. Finally, it should be noted that due to the weak coupling implied by the low  $\lambda$ , the predicted value of  $T_c$  is highly sensitive to

the choice of  $\mu^*$  although the prediction that the material is superconducting is robust in the usual range of  $\mu^*$  from 0.10 to 0.15.

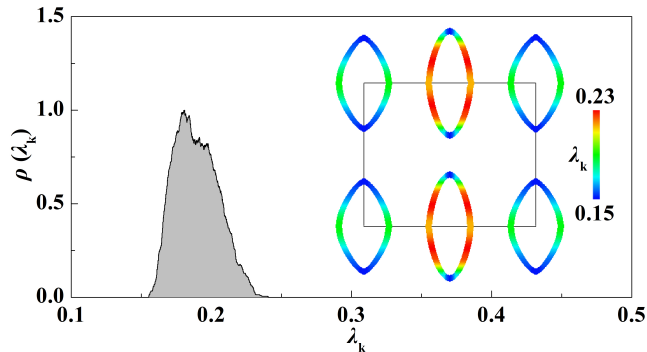


FIG. 8. Distribution of the EPC strength  $\lambda_{\mathbf{k}}$  of single-layer biphenylene. The data points correspond to electrons within  $\pm 200$  meV from the Fermi energy. Inset: Momentum-resolved EPC parameters  $\lambda_{\mathbf{k}}$  on the Fermi surface. The Brillouin zone is indicated by the solid lines.

We further investigated the superconductivity by calculations using the density functional theory for superconductors by solving the gap equation with the Superconducting-Toolkit package<sup>82,83</sup>:

$$\Delta_{n\mathbf{k}} = -\frac{1}{2} \sum_{n'\mathbf{k}'} \frac{K_{n\mathbf{k}n'\mathbf{k}'}^{el-el} + K_{n\mathbf{k}n'\mathbf{k}'}^{el-ph}}{Z_{n\mathbf{k}}} \frac{\Delta_{n'\mathbf{k}'}}{E_{n'\mathbf{k}'}} \times \tanh\left(\frac{\beta E_{n'\mathbf{k}'}}{2}\right), \quad (9)$$

where  $K_{n\mathbf{k}n'\mathbf{k}'}^{el-el}$ ,  $K_{n\mathbf{k}n'\mathbf{k}'}^{el-ph}$ , and  $Z_{n\mathbf{k}}$  are the electron-electron kernel, electron-phonon kernel and renormalization, respectively. As shown in Fig. 8, the calculated  $\lambda_{\mathbf{k}}$  has a significant anisotropy on the Fermi surface with values varying from 0.15 to 0.23. However, only one peak is in the distribution  $\rho(\lambda_{\mathbf{k}})$ , which implies that although there are two sheets of Fermi surface the material should be classified as a single gap superconductor<sup>28</sup>. The momentum-resolved EPC parameter  $\lambda_{n\mathbf{k}}$  on the Fermi surface is shown in the inset of Fig. 8. Comparing with the band structure in Fig. 2b and the Fermi surface plot in Fig. 3a, one observes that the larger values of  $\lambda_{\mathbf{k}}$  are on the Y-centered Fermi pockets dominated by the valence band. Overall, our calculated EPC  $\lambda = 0.19$  and  $T_c = 0.46$  K from the superconducting density functional calculation are in accord with the values ( $\mu^* = 0.1$ ,  $\lambda = 0.3$ ,  $T_c = 0.59$  K) from the averaging and McMillan-Allen-Dynes formula.

#### IV. CONCLUSIONS

In summary, we investigated the electronic structure and electron-phonon coupling of the recently synthesized  $sp^2$  carbon allotrope, single-layer biphenylene. We find that the Dirac cones in biphenylene sheet are of type-II and in pairs with opposite valued Berry curvature. The topological nature is confirmed by the presence of edge states and the non-zero

topological  $\mathbb{Z}_2$  invariant. We also find low temperature weak coupling single gap superconductivity. This arises from the combination of a very high logarithmically averaged phonon frequency, dominated by the in-plane vibrations, with a relatively low EPC constant  $\lambda$ . Thus monolayer biphenylene is predicted to be a topological superconductor and may therefore be a useful platform for studying the interplay of topological bands and superconductivity in an intrinsic material. It will therefore be of considerable interest to perform low temperature experimental studies searching for superconductivity in biphenylene and its monolayers.

#### ACKNOWLEDGMENTS

The authors acknowledge financial support from the National Natural Science Foundation of China (Grant Nos. 12074381, 12005230, 12104458, and 12074241), Foshan (Southern China) Institute for New Materials (Grant No. 2021AYF25021), Key Scientific and Technological Project of Henan Province (Grant No. 212102210577), and Science Foundation of Henan University of Technology (Grant No. 31401129). The numerical calculations were performed at Supercomputer Center of the China Spallation Neutron Source and Hefei advanced computing center. Theoretical work at the University of Missouri was supported by the U.S. Department of Energy, Award DE-SC0019114.

#### Appendix A

As shown in Fig. 9, the valence band (blue line) and the conduction band (red line) touch at the Dirac point with a tilted-over cone in energy-momentum space. In addition, the two bands along the  $\Gamma$ -Y line have slopes with the same sign, which is an intuitive criterion for type-II points<sup>84</sup>.

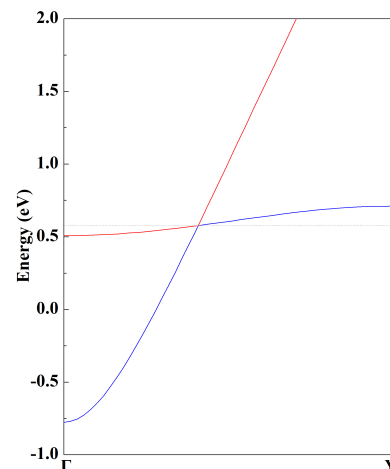


FIG. 9. The enlarged band structure along the  $\Gamma$ -Y line of the biphenylene monolayer. The blue and red lines highlight the valence band and conduction band of the biphenylene monolayer, respectively. The gray dot lines are the energy level of the Dirac points.

- \* [wangbt@ihep.ac.cn](mailto:wangbt@ihep.ac.cn)
- <sup>1</sup> Andreas Hirsch, “The era of carbon allotropes,” *Nat. Mater.* **9**, 868–871 (2010).
  - <sup>2</sup> P. R. Wallace, “The band theory of graphite,” *Phys. Rev.* **71**, 622–634 (1947).
  - <sup>3</sup> C.A. Brookes and E.J. Brookes, “Diamond in perspective: a review of mechanical properties of natural diamond,” *Diam. Relat. Mater.* **1**, 13–17 (1991).
  - <sup>4</sup> M.S. Dresselhaus, G. Dresselhaus, and R. Saito, “Physics of carbon nanotubes,” *Carbon* **33**, 883–891 (1995).
  - <sup>5</sup> Roger Taylor and David R. M. Walton, “The chemistry of fullerenes,” *Nature* **363**, 685–693 (1993).
  - <sup>6</sup> Andre Konstantin Geim, “Graphene: status and prospects,” *Science* **324**, 1530–1534 (2009).
  - <sup>7</sup> A. H. Castro Neto, F. Guinea, N. M. R. Peres, K. S. Novoselov, and A. K. Geim, “The electronic properties of graphene,” *Rev. Mod. Phys.* **81**, 109–162 (2009).
  - <sup>8</sup> Xu Du, Ivan Skachko, Anthony Barker, and Eva Y. Andrei, “Approaching ballistic transport in suspended graphene,” *Nat. Nanotech.* **3**, 491–495 (2008).
  - <sup>9</sup> C. L. Kane and E. J. Mele, “Quantum spin Hall effect in graphene,” *Phys. Rev. Lett.* **95**, 226801 (2005).
  - <sup>10</sup> C. W. J. Beenakker, “Colloquium: Andreev reflection and Klein tunneling in graphene,” *Rev. Mod. Phys.* **80**, 1337–1354 (2008).
  - <sup>11</sup> E. H. Hwang and S. Das Sarma, “Acoustic phonon scattering limited carrier mobility in two-dimensional extrinsic graphene,” *Phys. Rev. B* **77**, 115449 (2008).
  - <sup>12</sup> P. San-Jose, J. L. Lado, R. Aguado, F. Guinea, and J. Fernández-Rossier, “Majorana zero modes in graphene,” *Phys. Rev. X* **5**, 041042 (2015).
  - <sup>13</sup> Xiaowen Yu, Huhu Cheng, Miao Zhang, Yang Zhao, Liangti Qu, and Gaoquan Shi, “Graphene-based smart materials,” *Nat. Rev. Mater.* **2**, 1–13 (2017).
  - <sup>14</sup> Daniel Malko, Christian Neiss, Francesc Viñes, and Andreas Görling, “Competition for graphene: Graphynes with direction-dependent Dirac cones,” *Phys. Rev. Lett.* **108**, 086804 (2012).
  - <sup>15</sup> Zhenhai Wang, Xiang-Feng Zhou, Xiaoming Zhang, Qiang Zhu, Huafeng Dong, Mingwen Zhao, and Artem R. Oganov, “Phagraphene: A low-energy graphene allotrope composed of 5-6-7 carbon rings with distorted Dirac cones,” *Nano Lett.* **15**, 6182–6186 (2015).
  - <sup>16</sup> Xiaoming Zhang, Lin Wei, Jie Tan, and Mingwen Zhao, “Prediction of an ultrasoft graphene allotrope with Dirac cones,” *Carbon* **105**, 323–329 (2016).
  - <sup>17</sup> Li-Chun Xu, Ru-Zhi Wang, Mao-Sheng Miao, Xiao-Lin Wei, Yuan-Ping Chen, Hui Yan, Woon-Ming Lau, Li-Min Liu, and Yan-Ming Ma, “Two dimensional Dirac carbon allotropes from graphene,” *Nanoscale* **6**, 1113–1118 (2014).
  - <sup>18</sup> Xin Chen, Adrien Bouhon, Linyang Li, François M. Peeters, and Biplab Sanyal, “PAI-graphene: A new topological semimetallic two-dimensional carbon allotrope with highly tunable anisotropic Dirac cones,” *Carbon* **170**, 477–486 (2020).
  - <sup>19</sup> J Nagamatsu, N Nakagawa, T Muranaka, Y Zenitani, and J Akimitsu, “Superconductivity at 39 K in magnesium diboride,” *Nature* **410**, 63–64 (2001).
  - <sup>20</sup> J Kortus, I I Mazin, K D Belashchenko, V P Antropov, and L L Boyer, “Superconductivity of metallic boron in MgB<sub>2</sub>,” *Phys. Rev. Lett.* **86**, 4656 (2001).
  - <sup>21</sup> Y Kong, O V Dolgov, O Jepsen, and O K Andersen, “Electron-phonon interaction in the normal and superconducting states of MgB<sub>2</sub>,” *Phys. Rev. B* **64**, 020501(R) (2001).
  - <sup>22</sup> S. Souma, Y. Machida, T. Sato, T. Takahashi, H. Matsui, S. C. Wang, H. Ding, A. Kaminski, J. C. Campuzano, S. Sasaki, and K. Kadowaki, “The origin of multiple superconducting gaps in MgB<sub>2</sub>,” *Nature* **423**, 65–67 (2003).
  - <sup>23</sup> A F Hebard, M J Rosseinsky, R C Haddon, D W Murphy, S H Glarum, T T M Palstra, A P Ramirez, and A R Kortan, “Superconductivity at 18 K in potassium-doped C<sub>60</sub>,” *Nature* **350**, 600–601 (1991).
  - <sup>24</sup> Matthias Einenkel and Konstantin B. Efetov, “Possibility of superconductivity due to electron-phonon interaction in graphene,” *Phys. Rev. B* **84**, 214508 (2011).
  - <sup>25</sup> Bruno Uchoa and A. H. Castro Neto, “Superconducting states of pure and doped graphene,” *Phys. Rev. Lett.* **98**, 146801 (2007).
  - <sup>26</sup> Gianni Profeta, Matteo Calandra, and Francesco Mauri, “Phonon-mediated superconductivity in graphene by lithium deposition,” *Nat. Phys.* **8**, 131–134 (2012).
  - <sup>27</sup> Rahul Nandkishore, L. S. Levitov, and A. V. Chubukov, “Chiral superconductivity from repulsive interactions in doped graphene,” *Nat. Phys.* **8**, 158–163 (2012).
  - <sup>28</sup> Jing-Jing Zheng and E. R. Margine, “First-principles calculations of the superconducting properties in Li-decorated monolayer graphene within the anisotropic Migdal-Eliashberg formalism,” *Phys. Rev. B* **94**, 064509 (2016).
  - <sup>29</sup> Maximilian L. Kiesel, Christian Platt, Werner Hanke, Dmitry A. Abanin, and Ronny Thomale, “Competing many-body instabilities and unconventional superconductivity in graphene,” *Phys. Rev. B* **86**, 020507 (2012).
  - <sup>30</sup> E. R. Margine and Feliciano Giustino, “Two-gap superconductivity in heavily *n*-doped graphene: Ab initio migdal-eliashberg theory,” *Phys. Rev. B* **90**, 014518 (2014).
  - <sup>31</sup> Biao Lian, Zhijun Wang, and B. Andrei Bernevig, “Twisted bilayer graphene: A phonon-driven superconductor,” *Phys. Rev. Lett.* **122**, 257002 (2019).
  - <sup>32</sup> Fengcheng Wu, A. H. MacDonald, and Ivar Martin, “Theory of phonon-mediated superconductivity in twisted bilayer graphene,” *Phys. Rev. Lett.* **121**, 257001 (2018).
  - <sup>33</sup> B. M. Ludbrook, G. Levy, P. Nigge, M. Zonno, M. Schneider, D. J. Dvorak, C. N. Veenstra, S. Zhdanovich, D. Wong, P. Dosanjh, C. Straßer, A. Stöhr, S. Forti, C. R. Ast, U. Starke, and A. Damascelli, “Evidence for superconductivity in Li-decorated monolayer graphene,” *Proc. Natl. Acad. Sci.* **112**, 11795–11799 (2015).
  - <sup>34</sup> Satoru Ichinokura, Katsuaki Sugawara, Akari Takayama, Takashi Takahashi, and Shuji Hasegawa, “Superconducting calcium-intercalated bilayer graphene,” *ACS Nano* **10**, 2761–2765 (2016).
  - <sup>35</sup> J. Chapman, Y. Su, C. A. Howard, D. Kundys, A. N. Grigorenko, F. Guinea, A. K. Geim, I. V. Grigorieva, and R. R. Nair, “Superconductivity in Ca-doped graphene laminates,” *Sci. Rep.* **6**, 23254 (2016).
  - <sup>36</sup> E. R. Margine, Henry Lambert, and Feliciano Giustino, “Electron-phonon interaction and pairing mechanism in superconducting Ca-intercalated bilayer graphene,” *Sci. Rep.* **6**, 21414 (2016).
  - <sup>37</sup> S.-L. Yang, J. A. Sobota, C. A. Howard, C. J. Pickard, M. Hashimoto, D. H. Lu, S.-K. Mo, P. S. Kirchmann, and Z.-X. Shen, “Superconducting graphene sheets in CaC<sub>6</sub> enabled by phonon-mediated interband interactions,” *Nat. Commun.* **5**, 3493 (2014).
  - <sup>38</sup> Yi Luo, Chongdan Ren, Yujing Xu, Jin Yu, Sake Wang, and Minglei Sun, “A first principles investigation on the structural, mechanical, electronic, and catalytic properties of biphenylene,” *Sci. Rep.* **11**, 19008 (2021).



- <sup>39</sup> Florian Schlütter, Tomohiko Nishiuchi, Volker Enkelmann, and Klaus Müllen, “Octafunctionalized biphenylenes: Molecular precursors for isomeric graphene nanostructures,” *Angew. Chem. Int. Ed.* **53**, 1538–1542 (2014).
- <sup>40</sup> Pablo A. Denis and Federico Iribarne, “Hydrogen storage in doped biphenylene based sheets,” *Comput. Theor. Chem.* **1062**, 30–35 (2015).
- <sup>41</sup> David Ferguson, Debra J. Searles, and Marlies Hankel, “Biphenylene and phagraphene as lithium ion battery anode materials,” *ACS Appl. Mater. Interfaces* **9**, 20577–20584 (2017).
- <sup>42</sup> Qitang Fan, Linghao Yan, Matthias W. Tripp, Ondřej Krejčí, Stavrina Dimosthenous, Stefan R. Kachel, Mengyi Chen, Adam S. Foster, Ulrich Koert, Peter Liljeroth, and J. Michael Gottfried, “Biphenylene network: A nonbenzenoid carbon allotrope,” *Science* **372**, 852–856 (2021).
- <sup>43</sup> Mathew A Hudspeth, Brandon W Whitman, Veronica Barone, and Juan E Peralta, “Electronic properties of the biphenylene sheet and its one-dimensional derivatives,” *ACS Nano* **4**, 4565–4570 (2010).
- <sup>44</sup> Xin-Quan Wang, Han-Dong Li, and Jian-Tao Wang, “Prediction of a new two-dimensional metallic carbon allotrope,” *Phys. Chem. Chem. Phys.* **15**, 2024–2030 (2013).
- <sup>45</sup> Pablo A Denis, “Stability and electronic properties of biphenylene based functionalized nanoribbons and sheets,” *J. Phys. Chem. C* **118**, 24976–24982 (2014).
- <sup>46</sup> N. Troullier and José Luís Martins, “Efficient pseudopotentials for plane-wave calculations,” *Phys. Rev. B* **43**, 1993–2006 (1991).
- <sup>47</sup> Martin Fuchs and Matthias Scheffler, “Ab initio pseudopotentials for electronic structure calculations of poly-atomic systems using density-functional theory,” *Comput. Phys. Commun.* **119**, 67–98 (1999).
- <sup>48</sup> Paolo Giannozzi, Stefano Baroni, Nicola Bonini, Matteo Calandra, Roberto Car, Carlo Cavazzoni, Davide Ceresoli, Guido L Chiarotti, Matteo Cococcioni, Ismaila Dabo, Andrea Dal Corso, Stefano de Gironcoli, Stefano Fabris, Guido Fratesi, Ralph Gebauer, Uwe Gerstmann, Christos Gougoussis, Anton Kokalj, Michele Lazzeri, Layla Martin-Samos, Nicola Marzari, Francesco Mauri, Riccardo Mazzarello, Stefano Paolini, Alfredo Pasquarello, Lorenzo Paulatto, Carlo Sbraccia, Sandro Scandolo, Gabriele Sclauzero, Ari P Seitsonen, Alexander Smogunov, Paolo Umari, and Renata M Wentzcovitch, “Quantum ESPRESSO: a modular and open-source software project for quantum simulations of materials,” *J. Phys.: Condens. Matter.* **21**, 395502 (2009).
- <sup>49</sup> P Giannozzi, O Andreussi, T Brumme, O Bunau, M Buongiorno Nardelli, M Calandra, R Car, C Cavazzoni, D Ceresoli, M Cococcioni, N Colonna, I Carnimeo, A Dal Corso, S de Gironcoli, P Delugas, R A DiStasio Jr, A Ferretti, A Floris, G Fratesi, G Fugallo, R Gebauer, U Gerstmann, F Giustino, T Gorni, J Jia, M Kawamura, H-Y Ko, A Kokalj, E Küçükbenli, M Lazzeri, M Marsili, N Marzari, F Mauri, N L Nguyen, H-V Nguyen, A Otero de-la Roza, L Paulatto, S Poncé, D Rocca, R Sabatini, B Santra, M Schlipf, A P Seitsonen, A Smogunov, I Timrov, T Thonhauser, P Umari, N Vast, X Wu, and S Baroni, “Advanced capabilities for materials modelling with Quantum ESPRESSO,” *J. Phys.: Condens. Matter.* **29**, 465901 (2017).
- <sup>50</sup> Hendrik J. Monkhorst and James D. Pack, “Special points for Brillouin-zone integrations,” *Phys. Rev. B* **13**, 5188–5192 (1976).
- <sup>51</sup> Stefano Baroni, Stefano De Gironcoli, Andrea Dal Corso, and Paolo Giannozzi, “Phonons and related crystal properties from density-functional perturbation theory,” *Rev. Mod. Phys.* **73**, 515 (2001).
- <sup>52</sup> Göran Grimvall, *The electron-phonon interaction in metals*, Vol. 8 (North-Holland Amsterdam, 1981).
- <sup>53</sup> Feliciano Giustino, “Electron-phonon interactions from first principles,” *Rev. Mod. Phys.* **89**, 015003 (2017).
- <sup>54</sup> Ph B Allen and RC Dynes, “Transition temperature of strongly coupled superconductors reanalyzed,” *Phys. Rev. B* **12**, 905 (1975).
- <sup>55</sup> GM Eliashberg, “Interactions between electrons and lattice vibrations in a superconductor,” *Sov. Phys. JETP* **11**, 696–702 (1960).
- <sup>56</sup> P. B. Allen and R. C. Dynes, “Transition temperature of strongly coupled superconductors reanalyzed,” *Phys. Rev. B* **12**, 905–922 (1975).
- <sup>57</sup> Nicola Marzari, Arash A. Mostofi, Jonathan R. Yates, Ivo Souza, and David Vanderbilt, “Maximally localized Wannier functions: Theory and applications,” *Rev. Mod. Phys.* **84**, 1419–1475 (2012).
- <sup>58</sup> Arash A. Mostofi, Jonathan R. Yates, Giovanni Pizzi, Young-Su Lee, Ivo Souza, David Vanderbilt, and Nicola Marzari, “An updated version of wannier90: A tool for obtaining maximally-localised Wannier functions,” *Comput. Phys. Commun.* **185**, 2309–2310 (2014).
- <sup>59</sup> Giovanni Pizzi, Valerio Vitale, Ryotaro Arita, Stefan Blügel, Frank Freimuth, Guillaume Géranton, Marco Gibertini, Dominik Gresch, Charles Johnson, Takashi Koretsune, Julen Ibañez-Azpiroz, Hyungjun Lee, Jae-Mo Lihm, Daniel Marchand, Antimo Marrazzo, Yuriy Mokrousov, Jamal I Mustafa, Yoshiro Nohara, Yusuke Nomura, Lorenzo Paulatto, Samuel Poncé, Thomas Ponweiser, Junfeng Qiao, Florian Thöle, Stefan S Tsirkin, Małgorzata Wierzbowska, Nicola Marzari, David Vanderbilt, Ivo Souza, Arash A Mostofi, and Jonathan R Yates, “Wannier90 as a community code: new features and applications,” *J. Phys.: Condens. Matter.* **32**, 165902 (2020).
- <sup>60</sup> M P Lopez Sancho, J M Lopez Sancho, J M L Sancho, and J Rubio, “Highly convergent schemes for the calculation of bulk and surface Green functions,” *J. Phys. F: Met. Phys.* **15**, 851–858 (1985).
- <sup>61</sup> QuanSheng Wu, ShengNan Zhang, Hai-Feng Song, Matthias Troyer, and Alexey A. Soluyanov, “WannierTools: An open-source software package for novel topological materials,” *Comput. Phys. Commun.* **224**, 405–416 (2018).
- <sup>62</sup> Mitsuaki Kawamura, “FermiSurfer: Fermi-surface viewer providing multiple representation schemes,” *Comp. Phys. Commun.* **239**, 197–203 (2019).
- <sup>63</sup> Obaidur Rahaman, Bohayra Mortazavi, Arezoo Dianat, Gianuario Cuniberti, and Timon Rabczuk, “Metamorphosis in carbon network: From penta-graphene to biphenylene under uniaxial tension,” *FlatChem* **1**, 65–73 (2017).
- <sup>64</sup> D J Singh and M H Du, “Density functional study of LaFeAsO<sub>1-x</sub>F<sub>x</sub>: A low carrier density superconductor near itinerant magnetism,” *Phys. Rev. Lett.* **100**, 237003 (2008).
- <sup>65</sup> J Sichau, M Prada, T Anlauf, T J Lyon, B Bosnjak, L Tiemann, and R H Blick, “Resonance microwave measurements of an intrinsic spin-orbit coupling gap in graphene: A possible indication of a topological state,” *Phys. Rev. Lett.* **122**, 046403 (2019).
- <sup>66</sup> Yugui Yao, Fei Ye, Xiao-Liang Qi, Shou-Cheng Zhang, and Zhong Fang, “Spin-orbit gap of graphene: First-principles calculations,” *Phys. Rev. B* **75**, 041401 (2007).
- <sup>67</sup> Liang Fu and C. L. Kane, “Topological insulators with inversion symmetry,” *Phys. Rev. B* **76**, 045302 (2007).
- <sup>68</sup> Liang Fu, C. L. Kane, and E. J. Mele, “Topological insulators in three dimensions,” *Phys. Rev. Lett.* **98**, 106803 (2007).
- <sup>69</sup> Di Xiao, Ming-Che Chang, and Qian Niu, “Berry phase effects on electronic properties,” *Rev. Mod. Phys.* **82**, 1959–2007 (2010).
- <sup>70</sup> J. Zak, “Berry’s phase for energy bands in solids,” *Phys. Rev. Lett.* **62**, 2747–2750 (1989).
- <sup>71</sup> Jiangxu Li, Lei Wang, Jiayi Liu, Ronghan Li, Zhenyu Zhang, and Xing-Qiu Chen, “Topological phonons in graphene,” *Phys. Rev.*



- B **101**, 081403 (2020).
- <sup>72</sup> J.L. Lado, N. García-Martínez, and J. Fernández-Rossier, “Edge states in graphene-like systems,” *Synth. Met.* **210**, 56–67 (2015).
- <sup>73</sup> Tobias Wassmann, Ari P. Seitsonen, A. Marco Saitta, Michele Lazzeri, and Francesco Mauri, “Structure, stability, edge states, and aromaticity of graphene ribbons,” *Phys. Rev. Lett.* **101**, 096402 (2008).
- <sup>74</sup> Harish P. Veeravenkata and Ankit Jain, “Density functional theory driven phononic thermal conductivity prediction of biphenylene: A comparison with graphene,” *Carbon* **183**, 893–898 (2021).
- <sup>75</sup> Penghua Ying, Ting Liang, Yao Du, Jin Zhang, Xiaoliang Zeng, and Zheng Zhong, “Thermal transport in planar  $sp^2$ -hybridized carbon allotropes: A comparative study of biphenylene network, pentaheptite and graphene,” *Int. J. Heat Mass Transf.* **183**, 122060 (2022).
- <sup>76</sup> Peng-Fei Liu, Tao Bo, Juping Xu, Wen Yin, Junrong Zhang, Fangwei Wang, Olle Eriksson, and Bao-Tian Wang, “First-principles calculations of the ultralow thermal conductivity in two-dimensional group-IV selenides,” *Phys. Rev. B* **98**, 235426 (2018).
- <sup>77</sup> Peng-Fei Liu, Tao Bo, Zhifeng Liu, Olle Eriksson, Fangwei Wang, Jijun Zhao, and Bao-Tian Wang, “Hexagonal  $M_2C_3$  ( $M = As, Sb, and Bi$ ) monolayers: new functional materials with desirable band gaps and ultrahigh carrier mobility,” *J. Mater. Chem. C* **6**, 12689–12697 (2018).
- <sup>78</sup> Luo Yan, Peng-Fei Liu, Tao Bo, Junrong Zhang, Ming-Hua Tang, Yong-Guang Xiao, and Bao-Tian Wang, “Emergence of superconductivity in a dirac nodal-line  $Cu_2Si$  monolayer: ab initio calculations,” *J. Mater. Chem. C* **7**, 10926–10932 (2019).
- <sup>79</sup> Miao Gao, Qi-Zhi Li, Xun-Wang Yan, and Jun Wang, “Prediction of phonon-mediated superconductivity in borophene,” *Phys. Rev. B* **95**, 024505 (2017).
- <sup>80</sup> Luo Yan, Peng-Fei Liu, Hengtao Li, Yong Tang, Junjie He, Xingyong Huang, Bao-Tian Wang, and Liujiang Zhou, “Theoretical dissection of superconductivity in two-dimensional honeycomb borophene oxide  $B_2O$  crystal with a high stability,” *npj Comput. Mater.* **6**, 94 (2020).
- <sup>81</sup> Xiaoming Zhang, Yinong Zhou, Bin Cui, Mingwen Zhao, and Feng Liu, “Theoretical discovery of a superconducting two-dimensional metal-organic framework,” *Nano Lett.* **17**, 6166–6170 (2017).
- <sup>82</sup> <http://sctk.osdn.jp/>.
- <sup>83</sup> Mitsuaki Kawamura, Ryosuke Akashi, and Shinji Tsuneyuki, “Anisotropic superconducting gaps in  $YNi_2B_2C$ : A first-principles investigation,” *Phys. Rev. B* **95**, 054506 (2017).
- <sup>84</sup> Si Li, Zhi-Ming Yu, Yugui Yao, and Shengyuan A. Yang, “Type-II topological metals,” *Front. Phys.* **15**, 43201 (2020).